Simplified Control Technique for High-Power-Factor Flyback Cuk and Sepic Rectifiers Operating in CCM

Simone Buso, *Member, IEEE*, Giorgio Spiazzi, *Member, IEEE*, and Donato Tagliavia

***Abstract*—Control techniques for high-power-factor rectifiers which do not need input voltage sensing are gaining considerable attention due to their simpler implementation and inherently superior stability, as compared to conventional average or peak current mode control. Among these, the solutions based on the integration of a current signal (switch, diode, or inductor current) provide an inherent noise immunity, which makes them further appealing. This paper proposes a simple implementation of one such control technique for high-power-factor flyback, Cuk, or Sepic rectifiers, which, while still retaining a high power factor, further reduces the control complexity, thus making the solution very attractive for smart-power integration. A 200-W flyback rectifier with the proposed control technique was implemented and tested. The achieved results are in good agreement with the expected performance.**

***Index Terms*—Control systems, high-power-factor rectifiers, smart power.**

I. Introduction

RECENTLY, control techniques for high-power-factor rectifiers operating in continuous conduction mode (CCM), which avoid the input voltage sensing, have received great attention due to their advantages, in terms of control complexity, compared to the well-known average or peak current mode control. In particular, the absence of the multiplier/divider and of the current error amplifier, together with the inherent stability of the current loop are the main advantages of these solutions, with respect to the standard controllers. In many of the presented solutions, suitable nonlinear carrier (NLC) waveforms are utilized together with the switch, diode, or inductor current sensing in order to achieve high power factor [1]–[3]. Such NLC waveforms are derived based on the steady-state voltage conversion ratio and, thus, depend on the converter topology and on which current is sensed. In other cases, a linear negative ramp carrier is employed as proposed in [4] and [5] with the aim of simplifying the carrier generator circuit. The latter solutions allow one to derive unity power factor flyback rectifiers only by complex manipulation of the converter current signal. For example, a double integral of the switch current is proposed in [4]–[6] with different possible implementations.

Paper IPCSD 00–026, presented at the 1999 Industry Applications Society Annual Meeting, Phoenix, AZ, October 3–7, and approved for publication in the IEEE TRANSACTIONS ON INDUSTRY APPLICATIONS by the Industrial Power Converter Committee of the IEEE Industry Applications Society. Manuscript submitted for review June 1, 1999 and released for publication May 15, 2000.

S. Buso and G. Spiazzi are with the Department of Electronics and Informatics, University of Padova, 35131 Padova, Italy (e-mail: simone.buso@dei.unipd.it; giorgio.spiazzi@dei.unipd.it).

D. Tagliavia is with ST Microelectronics, 95121 Catania, Italy (e-mail: donato.tagliavia@st.com).

Publisher Item Identifier S 0093-9994(00)07612-X.

Not all of these solutions are able to achieve unity power factor and, in any case, all of them suffer for some degree of input current distortion in the case where the converter operates in the discontinuous conduction mode (DCM) (which can occur only during a portion of the line half-period). However, this does not represent a big problem, since low-frequency harmonic standards like IEC 1000-3-2 allow a certain degree of current distortion, which simplifies the power-factor corrector (PFC) design, especially at low power levels (Class A equipment). The modest residual input current distortion is, in any case, abundantly below the limits, considering also the reduced power levels achievable with the considered converter topologies.

In this paper, a rugged and robust control technique for flyback, Cuk, and Sepic rectifiers operating in CCM is proposed, which basically consists of a simplification of the control approach presented in [4]–[6]. Its final reduced complexity makes it very attractive for the integration in a smart-power integrated circuit (IC), comprising both the control circuitry and the power switch. The availability of such an IC will make it possible to develop cost-effective and compact PFC designs, with a minimum number of components on the printed circuit board.

In Section II, the NLC control technique is reviewed together with its variations, while in Section III, some general features regarding the technology which is going to be employed for the future integration of the control circuit and the power switch on the same silicon chip are discussed.

In Section IV, a detailed description of the control implementation is presented, where the peculiarities of the integration technology and the available design options are discussed. Finally, some experimental results from a 200-W flyback prototype, built using discrete components, are shown in Section V. These demonstrate the validity of the proposed approach.

II. Review of NLC Control for Flyback Rectifiers

This control technique was originally presented by Maksimovic *et al.* for the boost PFC in [1] and extended to flyback, Cuk, and Sepic rectifiers in [2].

Let us refer to Fig. 1(a), which shows the basic scheme of a high- power-factor rectifier based on the flyback topology, together with a general NLC controller, whose operation is based on the switch current sensing. The latter is preferred over the diode current information since it allows an easy switch protection implementation. The average input current is given by

$$\bar{i}_g(\theta) = \frac{1}{T_S}\int_0^{dT_S} i_g(\tau)\,d\tau = \frac{u_g(\theta)}{R_e} \tag{1}$$

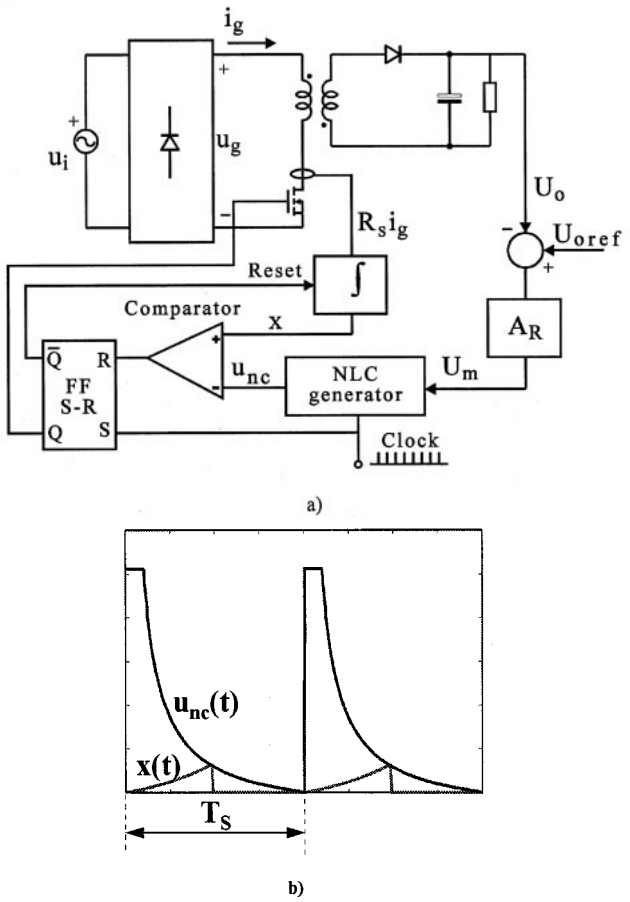

Fig. 1. (a) High-power-factor flyback rectifier with a general nonlinear carrier control. (b) Main controller waveforms.

where the second equality states that, in order to obtain a unity power factor, the absorbed current must be proportional to the input voltage (R_e is the emulated resistance, which depends on actual power delivered to the load). Note that overlined variables are averaged in a switching period and, therefore, are, in general, a function of the instantaneous line angle θ. Assuming CCM of operation, the voltage conversion ratio $m(\theta)$ is given by

$$m(\theta) = \frac{U_o}{u_g(\theta)} = n\frac{d(\theta)}{1-d(\theta)} \tag{2}$$

where $n = N_2/N_1$ is the transformer turns ratio.

By deriving $u_g(\theta)$ from (2) and substituting it into (1), we obtain

$$\frac{R_S}{T_S}\int_0^{dT_S} i_g(\tau)\,d\tau = \frac{R_S}{R_e}\frac{U_o}{n}\left(\frac{1-d(\theta)}{d(\theta)}\right) = U_m\left(\frac{1-d(\theta)}{d(\theta)}\right) \tag{3}$$

where R_s is the equivalent current-sensing resistance.

In (3), the emulated resistance R_e can be varied by the control signal U_m produced by the outer voltage feedback loop [see Fig. 1(a)]. In the steady state, $R_e = U_{g\text{peak}}^2/2P_o$, as can be derived from the converter power balance (unity efficiency assumed) while the control signal is $U_m = (R_S/R_e)(U_o/n) = 2nM^2R_SI_o$, where $M = U_o/(n\cdot U_{g\text{peak}})$. Since the duty cycle d is defined as T_{on}/T_s, (3) can be written as

$$\frac{R_S}{T_S}\int_0^t i_g(\tau)\,d\tau = U_m\left(1-\frac{t}{T_S}\right)\frac{T_S}{t} = u_{nc}(t) \tag{4}$$

where the first equality holds for $t = T_{\text{on}}$. Thus, the control strategy is as follows. A clock signal determines the switch turn-on instant, while the instant of turn-off is derived by comparing the integral of the switch current with the nonlinear carrier waveform $u_{nc}(t)$ given by the right-hand side of (4) (trailing-edge control). It is important to note that the same control approach can also be used with Cuk and Sepic rectifiers since they have the same voltage conversion ratio and the average switch current is equal to the average input current. The NLC control scheme is shown in Fig. 1(a), and its main waveforms are reported in Fig. 1(b).

As we can see, such control does not need any input voltage sensing nor multiplier/divider and current error amplifier. However, the generation of the exact nonlinear carrier signal $u_{nc}(t)$ is not straightforward.

In Section IV, a simplified control strategy is proposed which allows the minimization of the controller complexity at the expense of only a little increase in the input current harmonic distortion. As will be explained in the following, this is one of the main concerns in the design of the smart-power IC we are aiming at. Prior to that, in the following section, some general issues regarding the integration technology are presented.

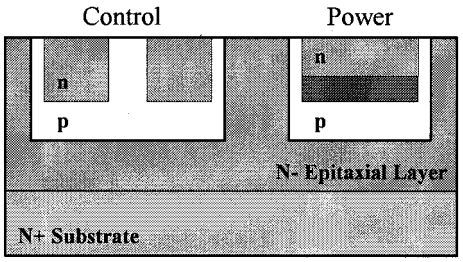

Fig. 2. VIPower technology.

III. VIPower M3 Technology

The reference technology for the application this paper deals with is the VIPower M3 technology developed by ST Microelectronics, Catania, Italy. This technology allows the integration on a single chip of a new type of power device, called *emitter switching*, and of all the required protection and control circuitry. As shown in Fig. 2, the control part is, at least in static conditions, electrically isolated from the power device part of the IC by means of reverse-biased p–n junctions. In the M3 level of the VIPower technology, a BCD-based control circuit can be implemented, where bipolar (both NPN and PNP), CMOS, and DMOS devices can be employed. The typical operating voltage is about 25 V.

Based on the thickness and resistivity of the N-epitaxial layer, the voltage rating of the power stage can range from 400 to 1500

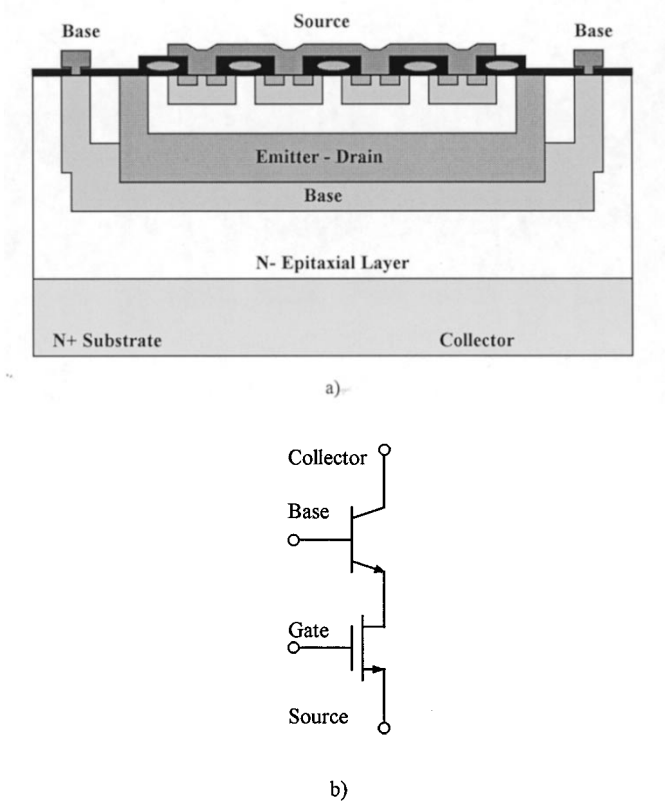

Fig. 3. Emitter switching device. (a) Schematic of device structure. (b) Equivalent circuit.

V. The maximum current level, depending on the size of the power stage, can reach 10 ÷ 15 A.

Fig. 3 shows the typical emitter switching structure. As can be seen, even if in Fig. 3(b) the emitter switching is represented as an equivalent series connection of two discrete devices, the actual power device is made up of the combination in a *sandwich* structure of a high-voltage bipolar NPN transistor and a low-voltage DMOS transistor. It is worth noting that this solution allows the integration of the DMOS inside the emitter area of the bipolar junction transistor (BJT), which implies that the used silicon area is that due only to the bipolar device. Moreover, the emitter of the bipolar device also represents the drain of the DMOS. This connection is buried inside the component and, therefore, a much shorter current path, compared with the series connection of two discrete devices, is achieved.

Finally, a key feature of this device is the minimization of the storage time in the bipolar component at turn-off, which gives to the emitter switching a quite high switching speed, comparable to that of a power MOSFet. This effect is achieved by giving a suitable discharge path to the base current which, at turn-off, is instantaneously made equal to the collector current by the quick opening of the DMOS transistor. Being as high as the collector current, the turn-off base current very quickly sweeps the accumulated charge off the bipolar transistor base, determining a very fast turn-off of the bipolar switch. Because of this structure, which implies an instantaneous turn-off of the BJT emitter current, no "tail" effects on the turn-off current are observed and the power dissipation during the transition remains well controlled.

IV. Proposed Control Implementation

The exact hyperbolic waveform $u_{nc}(t)$, derived from (4) in Section II, can be actually well approximated by a clamped exponential waveform, as proposed in [2]; however, its hardware implementation still requires a sample-and-hold circuit and an extra capacitor, whose discharge voltage provides the desired exponential waveform.

A different implementation can be derived by rearranging (4), as shown in the following:

$$\frac{t}{T_S}\frac{R_S}{T_S}\int_0^t i_g(\tau)\,d\tau = U_m\left(1-\frac{t}{T_S}\right) \tag{5}$$

where, again, the equality holds at the instant $t = T_{\rm on}$.

Here, simply moving the term $d(\theta)$ from the right-hand to the left-hand side of (3), the carrier waveform becomes a simple linear decreasing ramp, whose amplitude is imposed by the output of the voltage error amplifier. The control's complexity is now limited to the generation of the left-hand term of (5). Actually, this can be seen as an increasing ramp having a variable amplitude, given by the average input current value in a particular switching period (or in the previous one, as proposed in [5]). Alternatively, it can be approximated by the double integration of the switch current (if the inductor current has a small relative ripple), as proposed in [4] and [6]. Both of these solutions, however, appear to be a little too complicated for a cost-effective and reliable smart-power IC. It is worth underlining that the solution we are presenting here is aimed at the implementation of a general-purpose and low-cost type of product and, therefore, our goal is to achieve a satisfactory performance level with the minimum control circuit complexity.

Moreover, the harmonic standards like IEC 1000-3-2, provided that a Class A input current waveform is achieved, allow a significant amount of current distortion, especially at the low power levels achievable with such a converter topology. Based on these considerations, a simple single switch current integration was chosen as an approximation of the left-hand side of (5).

Besides, since the control signal U_m is a slowly varying signal (the output voltage control loop has a bandwidth well below the line frequency), the negative slope ramp appearing on the right-hand side of (5) can be generated by integrating the control signal U_m itself, together with the current signal. According to this approach, the control equation can be rewritten as

$$U_m = \frac{1}{T_s}\int_0^t (R_s i_g(\tau) + U_m)\,d\tau = \frac{R_s}{T_s}\int_0^t i_g(\tau)\,d\tau + \frac{U_m}{T_s}\,t \tag{6}$$

where the right-hand side, which represents variable x of the scheme in Fig. 4, is equal to U_m only when $t = T_{\rm on}$, as it was for (4) and (5). This means that the equality of signal U_m with the right-hand side of (6), which is a function of U_m itself, gives the $T_{\rm on}$ which corresponds to an approximated PFC operation of the rectifier. The approximation lies in the simplification of the left-hand side of (5) with a single integral.

As a result, the control implementation modifies as shown in Fig. 4. As can be seen, only one integrator with reset is needed to perform the integration of the sum of the control signal U_m and the signal proportional to the switch current. The resulting

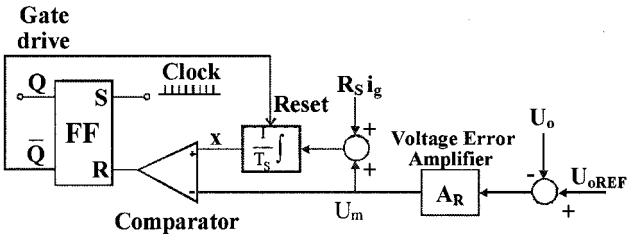

Fig. 4. Proposed control scheme.

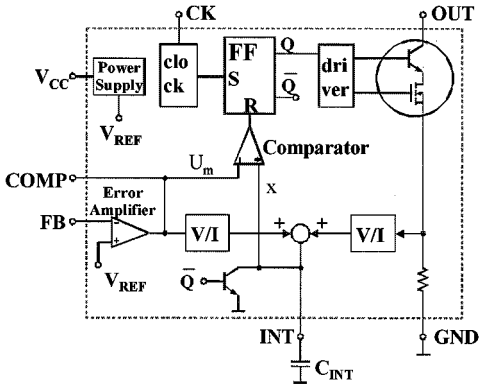

Fig. 5. Possible smart power integration scheme.

signal is compared with U_m, so as to derive the switch on time, as explained above. Note that this scheme is similar to that reported in [6], but, according to (6), a single integrator is used here instead of two.

Such a simple control approach, requiring very few blocks and having a potentially high immunity to the switching noise, thanks to the signal integration, is suitable for the implementation in the VIPower M3 technology. Besdies, the input voltage range of operation (90 ÷ 264 $V_{\rm rms}$) and the power rating of about 200 W for the typical application, imply a switch current stress of 6.5 A and a switch voltage stress of 800 V (taking into account the snubber operation in the flyback converter, not shown in Fig. 1), which are well within the power handling capability of this technology.

A possible block diagram of the smart power chip is given in Fig. 5. It is worth noting a peculiar feature of the M3 level of VIPower technology: the switch current is internally sensed by means of an integrated low-value resistor. The number of external components needed to complete the circuit is, therefore, limited to the minimum. The voltage drop across the sensing resistor is then converted into a current, which is finally integrated through the external capacitor $C_{\rm int}$ together with a current proportional to the output of the voltage error amplifier. Note that this second voltage-to-current converter can be avoided by using a transconductance error amplifier, also available in the technology blockset. The switch shown in the figure resets the integration capacitor every switching cycle. The other blocks shown in Fig. 5 (comparator, flip-flop, clock generator, etc.) are standard blocks, which can be found in any control IC and are, of course, also available in the VIPower technology. Note that a

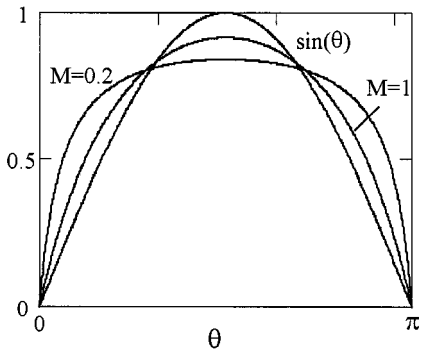

Fig. 6. Normalized input current waveforms at different conversion ratios M compared to the ideal sinusoidal waveform (same unity fundamental component amplitude).

cycle-by-cycle switch current protection can be easily added to the controller due to the internal current sensing. Finally, the internal power switch is the *emitter switching* structure described in the previous section.

We now complete the analysis of the control technique we have chosen, by investigating its intrinsic residual current distortion. In order to have an idea of the deviation of the average input current from the ideal sinusoidal one, we must observe that the chosen control strategy is equivalent to neglecting the term $d(\theta)$ at the denominator of the right-hand side of (3), that is to say,

$$\bar{i}_g(\theta) = \frac{U_m}{R_s}(1 - d(\theta)). \tag{7}$$

Rewriting (2), it is then possible to derive the expression of $d(\theta)$ as a function of $M = U_o/(n \cdot U_{g\rm peak})$ which turns out to be

$$d(\theta) = \frac{M}{|\sin(\theta)| + M}. \tag{8}$$

Finally, substituting (8) into (7) gives the following result:

$$\bar{i}_g(\theta) = \frac{U_m}{R_s}(1 - d(\theta)) = \frac{U_m}{R_S}\,\frac{|\sin(\theta)|}{|\sin(\theta)| + M}. \tag{9}$$

Fig. 6 reports the comparison between the ideal sinusoidal waveform and those given by (9) for two different conversion ratios M (all waveforms are normalized to a unity fundamental component). These waveforms have a harmonic content well below the Class-A limits of IEC 1000-3-2, at least up to some hundreds of watts. It is worth noting that a certain amount of input current distortion would be produced in any case, even if the exact nonlinear carrier signal was used. This happens because of the converter transition to DCM which takes place when the input voltage is close to zero. In any case, even if the converter operates at light load and in DCM for a large percentage of the line period, the performance remains fully acceptable, as will be shown in the following.

V. Experimental Results

A 200-W flyback rectifier, whose parameters are listed in Table I, was built using standard discrete components in order

TABLE I
CONVERTER PARAMETERS

Input Voltage U_g	90-260 V_{RMS}
Output Voltage U_o	48 V
Output Power P_o	200 W
Inductor L	1 mH
Filter Capacitor C	2200 μF
Switching Frequency f_s	50 kHz
Transformer Turns Ratio n	0.165

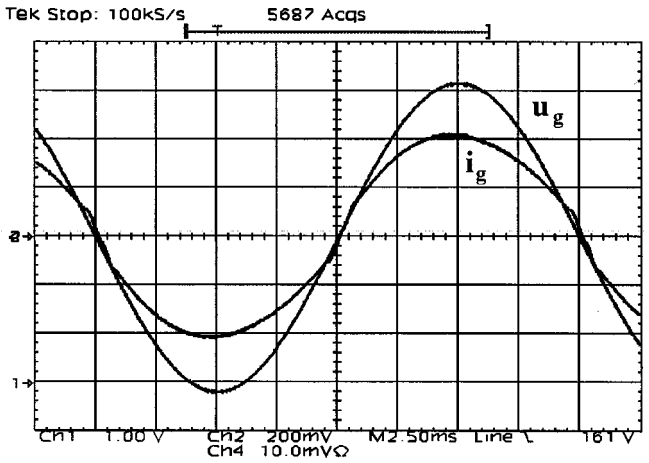

Fig. 7. Measured input voltage and filtered input current waveforms at $U_o = 48$ V, $P_o = 200$ W. (a) $U_g = 90\ V_{\rm rms}$, (40 V/div), I_g (2 A/div); (b) $U_g = 230\ V_{\rm rms}$, (100 V/div), I_g (1 A/div).

to test the performance of the proposed simplified control. The input current and voltage waveforms, in the nominal conditions, are shown in Fig. 7(a) for $U_g = 90\ V_{\rm rms}$, and in Fig. 7(b) for $U_g = 230\ V_{\rm rms}$.

As can be seen, measured input current harmonics, reported in Table II, are well below the limits, and correspond to a total

TABLE II
INPUT CURRENT HARMONICS FOR THE PROPOSED RECTIFIER AT $U_g = 230\ V_{\rm rms}$, $P_o = 200$ W

I_n	Analysis [mA_{rms}]	Simulation [mA_{rms}]		Measurement [mA_{rms}]	Class A limits [A_{rms}]
I_3	123	122	48.4	29	2.30
I_5	35.3	32.4	12.8	25	1.14
I_7	14.8	11.6	13.1	19	0.77
I_9	7.07	6.04	12.9	12	0.40
I_{11}	4.12	3.31	9.69	9	0.33
I_{13}	2.55	1.26	7.0	7	0.21
I_{15}	1.68	1.36	4.03	5	0.15
I_{17}	1.17	1.04	2.26	4	0.132
I_{19}	0.841	1.55	1.13	5	0.118
I_{21}	0.627	0.448	1.77	6	0.107

harmonic distortion (THD) for the input current slightly lower than 5%. Actually, as far as compliance with the standards is concerned, this control approach could be employed at power levels well beyond the value recommended for the flyback topology. Table II also includes the results coming from the theoretical analysis of the converter operation, based on (9), and from numerical simulations. As can be seen, a good agreement between simulation (left column) and theoretical analysis is achieved. As far as the experimental measurements are concerned, the small zero-crossing distortion of the line current causes an increase in the higher order harmonics (from the 15th on). The lower order harmonics, instead, do not show a satisfactory match with the ones resulting from analysis and simulation (left column). This is, at least partially, due to the effect of the additional low-pass filter ($RC = 10\ \mu$s), which is used in the experimental prototype to clean the switch current feedback signal. In practice, this tends to operate as an approximate second integration on the current signal which makes the resulting input current closer to the ideal sinusoidal waveform, as predicted by (5). To verify this, a second simulation (right column) has been performed including the effect of the low-pass filter. As can be seen, a significant improvement of the matching with the experimental results is achieved. Clearly, in the integrated implementation of the control circuit it will not be possible to include such a heavy low-pass filter, due to the limitation in the integration of high capacitor values. Therefore, results closer to the analytical ones should be expected.

Fig. 8 describes the light-load converter behavior. When the input power reduces to about 130 W, the converter operates in DCM for about 90% of the line period. This means that (2) is, in principle, no longer valid and the PFC operation is negatively affected. Anyway, as can be seen, the input current still exhibits an acceptable waveform, with a THD which is in the range of 10% and a harmonic content which is still well below the standard

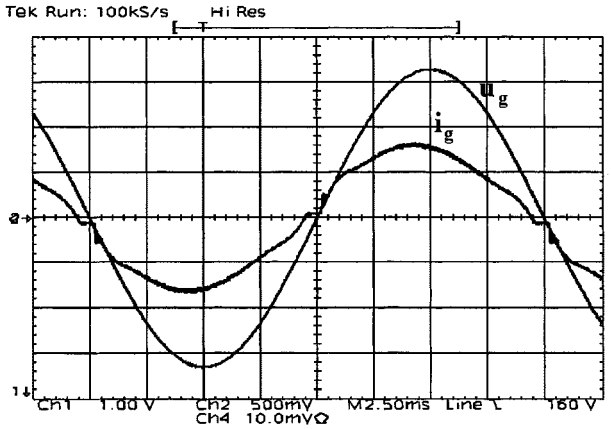

Fig. 8. Measured input voltage and filtered input current waveforms at $U_o = 48$ V, $P_{\rm in} = 130$ W *a:* $U_g = 230\ V_{\rm rms}$, (100 V/div), I_g (0.5 A/div).

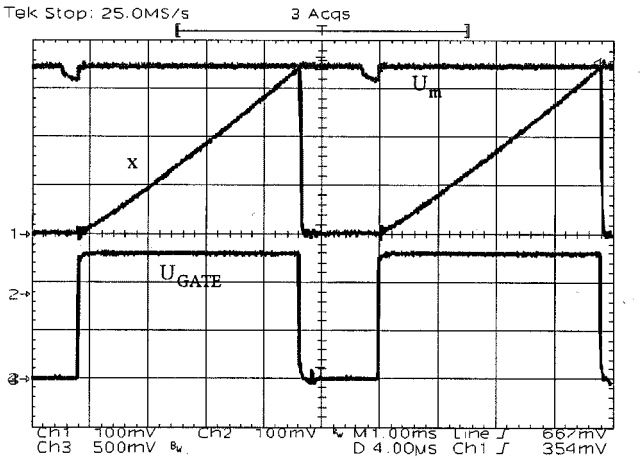

Fig. 9. Measured control waveforms. Current reference U_m (1 V/div), integral signal x (1 V/div), switch command $U_{\rm GATE}$ (5 V/div).

limits. It is worth remembering that, as far as the IEC standards are concerned, the behavior of the converter at reduced output power is not relevant, since all the tests have to be performed in the nominal conditions.

Finally, to describe the control circuit operation, in Fig. 9, the main control waveforms are depicted. As can be seen, the current reference is compared to the integral signal $x(t)$ according to the block diagram of Fig. 4. From this comparison, the switch command is generated. The small dip on the U_m signal is due to the discharge of the integrating capacitor $C_{\rm INT}$.

VI. Conclusions

This paper has presented a simple implementation of the NLC control technique for high-power-factor flyback, Cuk, or Sepic rectifiers, which makes the solution very attractive for smart-power integration, while still retaining a high power factor.

A 200-W flyback rectifier with the proposed control technique was implemented with discrete components and tested to evaluate the effectiveness of the control.

The results show good agreement with the expected performance. Further research and experimental work is in progress to test the fundamental blocks of the future smart-power IC, already available as single integrated circuits.

References

[1] D. Maksimovic, Y. Jang, and R. W. Erickson, "Nonlinear-carrier control for high-power-factor boost rectifiers," *IEEE Trans. Power Electron.*, vol. 11, pp. 578–584, July 1996.

[2] R. Zane and D. Maksimovic, "Nonlinear-carrier control for high-power-factor rectifiers based on flyback, cuk or sepic converters," in *Proc. IEEE APEC'96*, 1996, pp. 814–820.

[3] J. Hwang, A. Chee, and W. H. Ki, "New universal control methods for power factor correction and DC to DC converter applications," in *Proc. IEEE APEC'97*, 1997, pp. 59–65.

[4] J. P. Gegner and C. Q. Lee, "Linear peak current mode control: A simple active power factor correction control technique for continuous conduction mode," in *Proc. IEEE PESC'96*, 1996, pp. 196–202.

[5] J. R. Rajagopalan, P. Nora, and F. C. Lee, "A generalized technique for derivation of average current mode control laws for power factor correction without input voltage sensing," in *Proc. IEEE APEC'97*, 1997, pp. 81–87.

[6] Z. Lai and K. Smedley, "A family of power-factor-correction controllers," in *Proc. IEEE APEC'97*, 1997, pp. 66–73.

Simone Buso (M'98) was born in Padova, Italy, in 1968. He received the M.S. degree in electronic engineering and the Ph.D. degree in industrial electronics from the University of Padova, Padova, Italy, in 1992 and 1997, respectively.

Since 1993, he has been with the Power Electronics Laboratory, University of Padova, where he is currently a Researcher in the Department of Electronics and Informatics. His main research interests include dc/dc converters, smart power IC's, digital control, and robust control of power converters.

Giorgio Spiazzi (S'92–M'95) was born in Legnago, Italy, in 1962. He graduated with honors in electronic engineering and received the Ph.D. degree in industrial electronics and informatics from the University of Padova, Padova, Italy, in 1988 and 1993, respectively.

He is currently a Researcher in the Department of Electronics and Informatics, University of Padova. His main research interests are advanced control techniques for dc/dc converters, power-factor correctors, soft-switching techniques, and electromagnetic compatibility in power electronics.

Donato Tagliavia was born in Genoa, Italy, in 1955. He graduated as an Electronic Engineer from the University of Palermo, Palermo, Italy, in 1986.

In 1987, he was a Designer with Siemens Telecommunications, Milan, Italy. Since 1988, he has been with ST Microelectronics, Catania, Italy, first, as a Linear Voltage Regulator Designer and then as a Designer of electronic ignitions, SMPS, and industrial ICs. He is currently the Design Manager for automotive and industrial products using ST Microelectronics VIPower technologies.